Heavy Precipitation Impacts on Nitrogen Loading to the Gulf of Mexico in the 21st Century: Model projections under future climate scenarios

Jien Zhang[1], Chaoqun Lu[1*], William Crumpton[1], Christopher Jones[2], Hanqin Tian[3], Gabriele Villarini[2], Keith Schiling[4], David Green[1]

[1] Department of Ecology, Evolution, and Organismal Biology, Iowa State University, Ames, Iowa, USA

[2] IIHR—Hydroscience & Engineering, University of Iowa, Iowa City, Iowa, USA

[3] International Center for Climate and Global Change Research, School of Forestry and Wildlife Sciences, Auburn University, Auburn, Alabama, USA

[4] Iowa Geological Survey, Iowa City, Iowa, USA

[*] Correspondence author: C. L., clu@iastate.edu

Key Points:

- We examine the responses of nitrogen (N) loading from the Mississippi Atchafalaya River Basin (MARB) to future climate changes
- N loading from the MARB could increase by 30% under future climate scenarios, half of the increase would be driven by heavy precipitation
- Anthropogenic N input would be increasingly susceptible to leaching loss in the Midwest and Mississippi Alluvial Plain under future climate

***Abstract**:* While spatial heterogeneity of riverine nitrogen (N) loading is predominantly driven by the magnitude of basin-wide anthropogenic N input, the temporal dynamics of N loading are closely related to the amount and timing of precipitation. However, existing studies do not disentangle the contributions of heavy precipitation versus non-heavy precipitation predicted by future climate scenarios. Here we explore the potential responses of N loading from the Mississippi Atchafalaya River Basin to precipitation changes using a well-calibrated hydro-ecological model and Coupled Model Intercomparison Project Phase 5 climate projections under two Representative Concentration Pathway (RCP) scenarios. With present agricultural production and management practices, N loading could increase up to 30% by the end of the 21st century under future climate scenarios, half of which would be driven by heavy precipitation. Particularly, the RCP8.5 scenario, in which heavy precipitation and drought events become more frequent, would increase N loading disproportionately to projected increases in river discharge. N loading in spring would contribute 41% and 51% of annual N loading increase under the RCP4.5 and RCP8.5 scenarios, respectively, most of which is related to higher N yield due to increases in heavy precipitation. Anthropogenic N inputs would be increasingly susceptible to leaching loss in the Midwest and the Mississippi Alluvial Plain regions. Our results imply that future climate change alone, including more frequent and intense precipitation extremes, would increase N loading and intensify the eutrophication of the Gulf of Mexico over this coming century. More effective nutrient management interventions are needed to reverse this trend.

Keywords: Heavy precipitation, CMIP5, nitrogen loading, nitrogen leaching, Mississippi, the United States, Gulf of Mexico, water pollution

Plain Language Summary: Future climate change is expected to alter nutrient transport from land to rivers, which will have impacts on coastal ecosystems. The impacts of future

precipitation changes on nitrogen (N) loading, however, remain unclear. Based upon a well-tested hydro-ecological model, this work separates the roles of future heavy precipitation, non-heavy precipitation, and no-precipitation days in affecting N leaching loss and predicts the changes in N loading to the Gulf of Mexico. N loading is projected to increase by 30% under two climate scenarios (RCP4.5 and RCP8.5) by the end of the 21st century, half of which is likely driven by heavy precipitation. Future increases in spring heavy precipitation likely result in higher N leaching loss and increase N loading. Our results indicate that more effective nutrient reduction efforts will be needed to reach the reduction goals of N loading and hypoxia extent in the Gulf of Mexico.

1. Introduction

Increasing nutrient pollution in water bodies has become a global concern (Sinha et al., 2017). Excessive agricultural nitrogen (N) leached from soils and transported through river channels is a major driver of the formation and extent of hypoxic zones and algal blooms in estuaries and coastal waters (Howarth et al., 2000; Howarth & Marino, 2006). Since the 1960s, synthetic N fertilizer use has increased nine-fold globally (Lu & Tian, 2017), resulting in widely documented degradation of water quality (Evans et al., 2012; Grizzetti et al., 2011; Rabalais et al., 2007). Climate change is expected to increase the riverine N loading in many regions around the world (Howarth et al., 2006). Human-induced climate change has influenced the occurrence and the magnitude of extreme climatic events (National Academies of Sciences and Medicine, 2016). Therefore, understanding the response of land–to–aquatic N loading to extreme climatic events is therefore urgent and critical for better N management and assessment of progress toward reducing riverine N loading. Although previous studies have demonstrated the impacts of historical precipitation events on riverine N loading (Lu et al., 2020; Sinha et al., 2017; Tian et al., 2020), it remains unclear how future changes in the intensity and timing of precipitation events will affect riverine N loading.

Previous work has shown that year-to-year variations in precipitation amount drive over three-quarters of the inter-annual variability of N loading, and extreme precipitation events have been reported to only slightly influence N loading variations (Ballard et al., 2019; Donner & Kucharik, 2003; Lee et al., 2016; Sinha et al., 2017; Sinha & Michalak, 2016). However, other research shows that heavy precipitation could play an important role in enhancing nutrient loading under both historical and projected climate change conditions across scales (Carpenter et al., 2018; Zheng et al., 2020). Particularly, heavy rainfall after multiyear dry spells could

74 potentially increase N loading in the Susquehanna River Basin by 40% to 65%, leading to
75 enlarged hypoxic zones (Lee et al., 2016). Such a debate on the heavy precipitation impacts on N
76 loading arises primarily for two reasons: 1) existing research solely focused on the changes in
77 annual or monthly precipitation (Ballard et al., 2019; Sinha & Michalak, 2016), which did not
78 quantify the contributions of precipitations with different intensities (e.g., heavy precipitation
79 versus regular precipitation) on N loading at a daily time step, and 2) re-assembled natural
80 climate variability and continuity were often used to force factorial modeling experiments (Lee
81 et al., 2016), which did not necessarily reflect the real-world spatiotemporal changes in N
82 loading. These methodological limitations raise the concern that future N loading will be difficult
83 to predict without fully considering the various impacts of heavy precipitation and normal
84 precipitation in the coming decades.

85 Nutrient discharge from the Mississippi Atchafalaya River Basin (MARB) in the U.S. forms
86 the world's second-largest hypoxic zone in the receiving Gulf of Mexico (Thomas & Rahman,
87 2012). A previous study has shown that the MARB will likely experience large increases in
88 heavy precipitation in the coming century (Janssen et al., 2016). Here we quantify the impacts of
89 future precipitation events (e.g., rain and snow) with different intensities on riverine N loading
90 across the MARB using a daily time-step process-based hydro-ecological model, the Dynamic
91 Land Ecosystem Model (DLEM). The DLEM model considers the short- and long-term legacy
92 effects of precipitation on changes in water and N yield (Lu et al., 2020; Tian et al., 2020). In
93 DLEM, snowfall does not directly induce N leaching or loading but can affect soil moisture in
94 early spring due to snow melting, altering water yield (i.e., surface- and sub-surface runoff) as
95 well as N yield. Such processes may be triggered until the snow starts melting in DLEM. This
96 delayed effect will apply to the extreme snowfall as well. The goals of this study are to (1)

97 examine the patterns of future heavy precipitation (HP, daily precipitation is over the monthly
98 90^{th} percentiles) across the MARB under two climate scenarios (i.e., two representative
99 concentration pathways (RCP) scenarios, namely RCP4.5 and RCP8.5 as known as a "medium
100 stabilization scenario" and a " high baseline emission scenario", respectively, based on
101 greenhouse gas concentration trajectories; Fig. 1), (2) estimate the contributions of annual total
102 precipitation (TP), HP events, non-HP events, and no-precipitation days to water yield and N
103 yield across the MARB by the end of the century, and (3) identify the spatial hotspots of
104 increases in water yield and N yield driven by precipitation intensity change. We use the climate
105 projections generated by three CMIP5 models to force a hydro-ecological model, DLEM, that
106 incorporates land hydrological and biogeochemical processes with a networked river system.
107 Over the study period, the MARB exhibits no significant trends in annual precipitation under
108 future climate scenarios. This near-stationarity in annual precipitation exposes the role of daily
109 variations of precipitation intensity in driving N loading. Our analysis shows that HP is strongly
110 associated with increases in water and N yield by the end of the century.

111 **2. Methods**

112 **2.1 Data sources**

113 We obtained the future (defined as 2018-2099) daily climate data (temperature, precipitation, and
114 shortwave radiation) from the MACAv2-METDATA dataset
115 (http://www.climatologylab.org/maca.html) that is at 4 km × 4 km resolution for the U.S. They
116 were generated by three CMIP5 Earth System Models (ESMs) for the RCP4.5 and RCP8.5
117 scenarios (Table 1). Among the three ESMs, the HadGEM2-ES and the GFDL-ESM2G represent
118 the high and low bound of the projected global climate warming in the 21st century (Fig. 1a),
119 and the CNRM-CM5 is representative of the mid-values of equilibrium climate sensitivity in the

CMIP5 suite. The climate data were resampled to 5-arc min resolution using the inverse distance weighted interpolation to match the resolution of other input drivers used in this study. The historical climate data from 1979-2017 were downloaded from the MACA Training Data (https://climate.northwestknowledge.net/MACA/MACAtrainingdata.php). These training climate data, which were used to bias-correct and downscale the CMIP5 climate data in both the historical and future periods, were from the observation-based METDATA climate data developed by Abatzoglou (2013). The Multivariate Adapted Constructed Analogs (MACA) downscaling method exhibits well performance in temperature, humidity, wind, and precipitation due to its ability to jointly downscale temperature and dew point temperature and its use of analog patterns rather than interpolation (Abatzoglou & Brown, 2012). For the period from 1901 to 1978, we used the CRU-NARR climate data (Mesinger et al., 2006; Mitchell & Jones, 2005) to drive our model in the way as our previous studies (Lu et al., 2018, 2020; Yu et al., 2018). To develop a spatiotemporally consistent climate dataset, we adjusted the CRU-NARR climate data based on the MACA historical training data, namely the METDATA, by using a revised delta method (Liu et al., 2013). We first calculated a long-term average annual temperature and monthly temperature from 11 overlapping years (1979-1989) for the two climate data sources. The ratio of monthly temperature range between the two datasets was calculated as:

$$R = \left(T^{max}_{MACA-train} - T^{min}_{MACA-train}\right)/\left(T^{max}_{CRU-NARR} - T^{min}_{CRU-NARR}\right) \quad (1)$$

where $T^{max}_{MACA-train}$ and $T^{min}_{MACA-train}$ are respectively the maximum and minimum monthly temperatures from the MACA historical training climate data; $T^{max}_{CRU-NARR}$ and $T^{min}_{CRU-NARR}$ are respectively the maximum and minimum monthly temperatures from the CRU-NARR data from 1979-1989. Then we calculated the difference between the MACA annual temperature and the adjusted CRU-NARR annual temperature:

$$\Delta T = T_{CRU-NARR} \times R - T_{MACA-train} \quad (2)$$

where $T_{CRU-NARR}$ is the 11-year annual average temperature of the CRU-NARR data, R is the above-estimated ratio, and $T_{MACA-train}$ is the 11-year annual average temperature of the MACA-training data. The daily CRU-NARR temperature data from 1901-1978 were then adjusted as:

$$T_{adj,d} = T_d \times R - \Delta T \quad (3)$$

where T_d is the original CRU-NARR daily temperature, and $T_{adj,d}$ is the adjusted daily temperature that was used to drive simulations in this study. Through this modification, we not only modified the magnitude of CRU-NARR temperature but also reserved the annual amplitude signal from the MACA training data. The adjustment of radiation data was the same as the temperature data. Because the precipitation data is not continuous, we adjusted the precipitation by using the ratio (R') of annual average precipitation between the two data sources:

$$R' = (P^{sum}_{MACA-train}/P^{sum}_{CRU-NARR}) \quad (4)$$

where $P^{sum}_{MACA-train}$ and $P^{sum}_{CRU-NARR}$ are the annual average precipitation from 1979-1989 from the MACA-training data and the CRU-NARR data, respectively.

$$P_{adj,d} = P_d \times R' \quad (5)$$

where P_d is the original CRU-NARR daily precipitation, $P_{adj,d}$ is the adjusted CRU-NARR daily precipitation, and R' is the ratio of the annual total precipitation averaged from 1979-1989 calculated between the two climate data sources.

Table 1. CMIP5 models used for the simulations

Model Name	Original Resolution	Adjusted Resolution	Model Country	Historical Period	Future Period	References
CNRM-CM5	1.4° × 1.4°	0.083° × 0.083°	France	1961-2017	2018-2099	Voldoire et al., (2013)
GFDL-ESM2G	2.5° × 2.0°	0.083° × 0.083°	USA	1961-2017	2018-2099	Dunne et al., (2013)
HadGEM2-ES	1.88° × 1.25°	0.083° × 0.083°	UK	1961-2017	2018-2099	Collins et al., (2011)

Atmospheric CO_2 concentration for the 21st century was retrieved from the RCP Database (version 2.0) for the two examined scenarios (Clarke et al., 2007; Riahi et al., 2007; Smith & Wigley, 2006; Wise et al., 2009). Specifically, the RCP4.5 scenario represents the radiative forcing level stabilizes at 4.5 W m^{-2} before 2100 by utilizing a range of technologies and strategies for reducing greenhouse gas emissions (Thomson et al., 2011), and the RCP8.5 scenario stands for the radiative forcing level at 8.5 W m^{-2} characterized by high greenhouse gas concentration levels over time (Riahi et al., 2011).

The historical spatial N deposition data were obtained from the National Atmospheric Deposition Program (NADP) for the period 2000-2017 and extended to the period before 2000 by following the trend of global gridded N deposition data (Dentener, 2006; Wei et al., 2014). The time-series gridded data of historical crop-specific N fertilizer use rate, timing, and types used in this study are from Cao et al., (2018). Historical land use and land cover change data used in this study are from Yu & Lu, (2018), which includes time-varying gridded maps of crop types from 1850 to 2016. The dynamic extent of cropland distribution and interannual crop rotations are incorporated in our simulations through this historical land-use data. Manure data were obtained from Yang et al., (2016) at 5-arc min × 5-arc min resolution. DLEM also incorporates legume crops that fix atmospheric N (e.g., soybean and alfalfa). Biologically fixed

N is simulated and added into the soil available N pools for crop uptake and N transformation. N from biomass turnover and residual after harvesting also turns into soil N pools and poses legacy effects for crops planted next year. The details of model input data and model structure can be found in the Supplementary Information of Lu et al. (2020).

2.2 Partitioning precipitation into heavy, non-heavy, and no-precipitation conditions

To partition precipitation events into "heavy", "non-heavy", and "no-precipitation" conditions, we defined heavy precipitation when daily precipitation is over the monthly 90^{th} percentiles. This definition allows spatial comparison across a large region and accounts for seasonality (Zhang et al., 2016). For easy comparison with extreme climate indices, the monthly 90^{th} percentiles were estimated using all daily precipitation from days with precipitation greater than or equal to 1 mm in each month over the climatological baseline period 1961–1990. HP is identified at the grid cell level when the monthly 90^{th} percentile threshold was surpassed. As a result, the days with precipitation less than the 90^{th} percentiles but larger than 1 mm are defined as non-heavy precipitation days. The days with precipitation less than or equal to 1 mm are defined as no-precipitation days.

2.3 Model descriptions

Water and N yield: We used an improved version of the Dynamic Land Ecosystem Model (DLEM, version 2.0) that was developed to explicitly model carbon and N cycling, water balances, vegetation structure and growth, and senescence dynamics of managed ecosystems (Liu et al., 2013; Lu et al., 2018; Tian et al., 2010; Yu et al., 2020). Particularly, the DLEM is capable of simulating water flow and N fluxes from land ecosystems (crops, grasslands, forests, etc.) to streams and rivers. The N considered in DLEM includes dissolved organic N (DON),

dissolved inorganic N (DIN: NO_3-N and NH_4-N), and particulate organic N (PON). Since DIN constitutes over two-thirds of total N (TN) loading to the Northern Gulf of Mexico (Aulenbach et al., 2007; Scavia et al., 2017), we only quantified daily fluxes of DIN leaching and loading in this study. The representations of DIN leaching in DLEM are shown as following equations.

$$L_{NH4} = av_{NH4} \times Dis_{NH4} \times \frac{q_{srun} + q_{drain}}{W + q_{srun} + q_{drain}} / b_{NH4} \quad (6)$$

$$L_{NO3} = av_{NO3} \times Dis_{N03} \times \frac{q_{srun} + q_{drain}}{W + q_{srun} + q_{drain}} / b_{NO3} \quad (7)$$

where L_{NH4} and L_{NO3} are ammonia and nitrate leaching rates, av_{NH4} and av_{NO3} are soil available ammonia and nitrate, q_{srun} and q_{drain} are surface and sub-surface runoff, W is soil moisture content, and b_{NH4} and b_{NO3} are plant-dependent parameters, representing the soil buffer effect of available N. Dis_{NH4} and Dis_{N03} are dissolving efficiency coefficients for NH_4 and NO_3, respectively, which are tuned in the model (by default it is 0.2 for NH_4-N and 1 for NO_3-N). The daily change in soil NH_4-N and NO_3-N pools is determined by the difference between N input (e.g., N deposition, N fertilizer use, manure N, biological N fixation) and N output (plant N uptake, nitrous gas emission, N leaching, and N loss due to other unknown pathways). The internal N transformation due to mineralization, immobilization, nitrification, and denitrification also contributes to partition N into reduced and oxidized inorganic N pools and organic N pools.

In DLEM, leached N is delivered from the land to water bodies along with water movement. The daily lateral fluxes of both water (e.g., surface runoff and drainage runoff) and N enter two logical water pools, namely surface water pool and drainage water pool, before flowing into streams and lakes. The simulating time step for water flux from the land to the water pools is 30-minute. The N fluxes entering into the two pools are calculated based on allocation ratios that are

223 determined by the surface runoff and drainage runoff. The details of the calculation can be found
224 in Lu et al. (2020).

225 ***Land use and drought-induced crop mortality***: Each grid cell in DLEM is a cohort of up to four
226 natural plant functional types and one cropping system with its annual area percentage prescribed
227 by land use input data. In this work, the distribution and physiological properties of corn,
228 soybean, winter wheat, spring wheat, rice, and six other major crop types were specified across
229 the MARB. The model was parameterized to approach the observations of annual gross primary
230 production, and crop yields collected from multiple sites across the US (Lu et al., 2018; Yu et al.,
231 2019). To characterize the impacts of severe drought, we added a module to represent crop
232 mortality when drought intensity exceeds a threshold, which was based on air temperature and
233 soil water content (Mananze et al., 2019).

234 ***Agricultural management practices***: This version of DLEM also models the impacts of various
235 agricultural management practices, including applications of synthetic N fertilizer and manure on
236 crops, the effects of tile drainage on surface runoff, and the effects of technology innovations for
237 crop yield improvement (Lu et al., 2018). The time-series gridded data of historical crop-specific
238 N fertilizer use rate, timing, and types (e.g., NH_4-N and NO_3-N) were used to drive the DLEM
239 model. Specifically, N fertilizer is applied at four timings in DLEM, namely before-planting (in
240 spring before crop development), at-planting (in spring during crop planting), after-planting
241 (early summer shortly after crop early development), and after-harvesting (late fall). The four N
242 fertilizer timings are based on the phenology for each fertilized crop type. The amount and type
243 of applied N fertilizer at each timing are derived from the reconstructed fertilizer management
244 history data (Cao et al., 2018). Along with chemical N fertilizer data, manure N was applied
245 based on the prescribed input dataset. Our previous modeling study has confirmed that the

DLEM model captures the effects of N application amount and seasonality on the N yield and delivery from the MARB to the Gulf (Lu et al., 2020).

In DLEM, a percentage map of the tile-drained area is used to accelerate the water infiltration rate. The tile-drained land area percentage in a grid cell could range from 0 to 100% (Fig. S1). The sub-surface water flow is then accelerated by the adjusted infiltration rate, leading to faster runoff than the case without tile drainage. The impact of tile drainage was calibrated against the data from Malone et al., (2017). More details regarding tile drainage impacts can be found in Yu et al., (2018).

2.4 Model calibration and validation

We have calibrated the key parameters that regulate crop net primary productivity, soil organic C content, and water loss through evapotranspiration across multiple sites of the U.S. (Lu et al., 2018; Yu et al., 2018, 2019). In this study, we further calibrated parameters that control river discharge, soil N leaching, and riverine N loading. The simulated monthly streamflow and N loading to the Gulf of Mexico from 1980 to 2017 were validated by comparison with observed streamflow and N loading data obtained from the Mississippi River at St. Francisville, Louisiana (site ID 07373420) and Atchafalaya River at Melville, Louisiana (site ID 07381495) USGS monitoring sites and gauging stations (Fig. S2). The USGS-derived riverine NO_2-N, NO_3-N, and NH_4-N data were based on the LOADEST software package (https://water.usgs.gov/software/loadest/). In addition to the model validation at the river outlet to the Gulf, we also validated the model's performance in simulating annual river discharge and N export for eight major sub-basins of the MARB by comparing with the gauge-monitoring data obtained from the USGS (Table S1). DLEM estimates of river discharge and N load from these sub-basins are close to the USGS LOADEST estimates over years (Fig. S3). To further test the

model's performance in capturing peak streamflow and N loads, we compared the modeling results with the USGS LOADEST estimates across the eight sub-basins when extremely high flows were recorded during 1980-2015 (https://toxics.usgs.gov/pubs/of-2007-1080/flux.html). The top 5% of high flow months (defined as exceeding the 95th percentile of observed flow rates) at the eight gauging stations were used to represent the high flow months. The modeling estimates of discharge and N loading from these sub-basins are close to the USGS observations during extreme-flow months (Fig. S4). To remove the uncertainty derived from the LOADEST approach, our previous work has validated the DLEM-modeled daily river discharge and N concentration against the daily raw observations from the USGS (Lu et al., 2020). Overall, this model is able to reproduce the daily, monthly and inter-annual variations in water discharge and N loading from the eight sub-basins and the entire MARB.

2.5 Model simulations

We projected land-to-aquatic water yield and dissolved inorganic nitrogen (DIN) loads (including NH_4-N, NO_2-N, and NO_3-N) forward until 2099 using projected temperature, precipitation, and radiation from three CMIP5 ESMs under two RCP scenarios. All the simulations are forced by the transient climate from 1901 to 2099. Specifically, for the period 1901-2017, land use and land cover change, human agricultural management, and environmental drivers are based on the available databases introduced above. For the period 2018 to 2099, we kept all the environmental drivers but climate fixed to the 2017 level (e.g., N fertilizer input rates, N deposition, manure N rates, tile drainage, etc.). We also assumed that the land use pattern will not change for the post-2017 period. To keep crop rotations for the future period, we repeatedly used the crop type maps of 2016 and 2017 for the years after 2018 to represent an "unchanged" crop rotation practice for the future period. The set-ups of static land-use and "maintaining-the-

292 status" crop rotations allow us to distinguish and quantify the impacts of climate change and
293 extreme climatic events on N loading, assuming current agricultural practices remain unchanged
294 in the future. Furthermore, the simulation set-ups can highlight the potential drawbacks of
295 current agricultural management practices on improving water quality given future climatic
296 changes. We quantified N leaching to local waters at each grid as N yield (g N m^{-2} day^{-1}) and N
297 delivered to rivers and coastal areas after in-stream transfer and decay as N loading (Tg N day^{-1}).
298 Daily estimates were aggregated to the monthly or annual total for analysis and comparison
299 purposes.

2.6 Summarizing statistics

Changes in climate drivers (mainly precipitation-related), river discharge, N loading, water yield, and N yield were evaluated by the differences for these variables between the period 2070-2099 and the period 1988-2017. We reported changes in the mean annual precipitation (mm), heavy precipitation frequency (days), and aridity (days), along with changes in mean annual river discharge and N loading (%) and yield of water (km^3) and N (Tg). Aridity was represented by the indices of consecutive dry days (CDD), including annual total CDD, the longest CDD event, and the number of CDD events.

3. Results and Discussion

3.1 Changes in Precipitation in the MARB during the 21st Century

We first examine the patterns of future HP across the MARB for both RCP scenarios. The 30-year average annual HP from 2070-2099 across the MARB under the two climate scenarios shows a west-to-east gradient, ranging from less than 100 mm yr^{-1} in the west to ~600 mm yr^{-1} in the east (Fig. S5). Although the annual TP is projected to remain relatively stable for both scenarios (Fig. 1b), the annual total HP in the MARB on average would likely increase by 8% (±5%) and 15% (±8%) by the end of this century under the RCP4.5 and RCP8.5 scenarios, respectively (Table S2). HP amount is likely to increase substantially across the Upper Mississippi and Ohio River Basins where N fertilizer is intensively used to maximize crop yields of the U.S. Corn Belt region (generally referring to Minnesota, Illinois, Indiana, Iowa, Nebraska, and Ohio) (Fig. 2a-d). Only a small portion of the area lying within the southern MARB is projected to experience a decrease (< -50 mm yr^{-1}) in HP amount under the examined scenarios (Fig. 2c,d). However, the standard deviation (STD) of annual HP change shows a high variation

(60-90 mm yr^{-1}) in the southern area of the MARB among the three CMIP5 models (Fig. 2e,f). The spatial patterns of STD indicate that the predicted HP in this region has a larger uncertainty under both RCP scenarios, compared with the rest of MARB where the annual total HP STD is overall less than 60 mm yr^{-1} (Fig. 2e,f). We further find that, between the two climate scenarios, the RCP8.5 scenario shows a larger spatial extent with HP increase > 50 mm yr^{-1} than the RCP4.5 scenario (Fig. 2c-d), despite an overall similar small increase in the number of HP events found in both scenarios (Fig. S6 and Table S2).

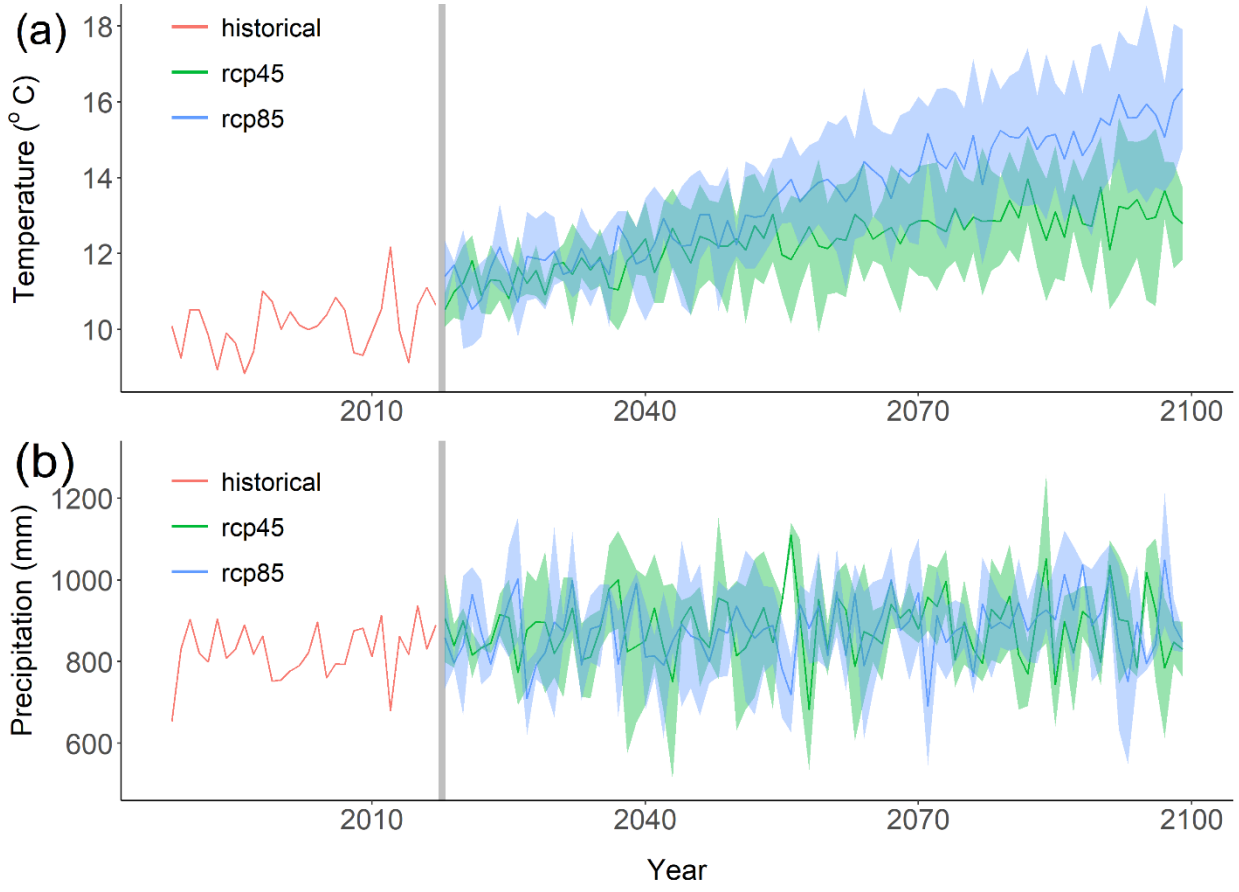

Figure 1. Mean annual temperature (**a**) and annual total precipitation (**b**) in the MARB for the historical period (1988-2017) from instrumental measurements by the METDATA climate data (Abatzoglou, 2013) and future period (2018-2099) projected by the three CMIP5 climate models.

333 The shaded area in **a** and **b** indicates the standard deviation across the three CMIP5 models. The

334 red curves indicate the historical period from 1988 to 2017.

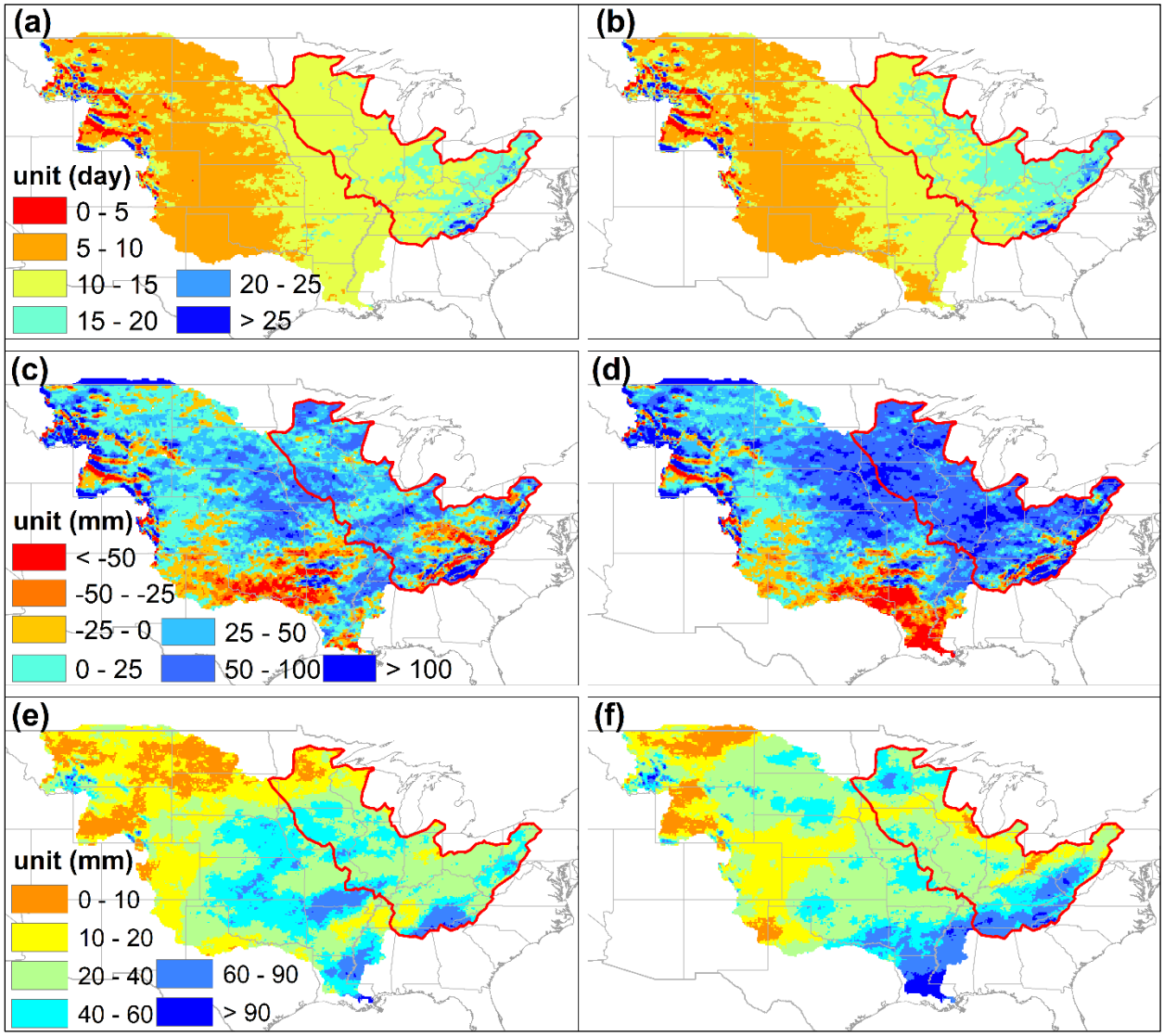

335

336 Figure 2. The number of days with heavy precipitation (HP) events each year averaged from

337 2070-2099 in the MARB under the RCP4.5 (**a**) and RCP8.5 (**b**) scenarios, the change of annual

338 HP amount (mm) in the MARB between the period 2070-2099 and the period 1988-2017 under

339 the RCP4.5 (**c**) and RCP8.5 (**d**) scenarios, and the standard deviation of the annual HP change

340 (mm) among three CMIP5 models under the RCP4.5 (**e**) and RCP8.5 (**f**) scenarios. The red

outlines in sub-figures highlight the upper-, mid-Mississippi River Basins, and the Ohio River Basin.

3.2 Impacts of Future Precipitation Change on Water Yield and Nitrogen Loss in the MARB

Forced by climate prediction data from three CMIP5 models along with present-day agricultural practices and N fertilizer inputs, our simulation indicates that the river discharge is projected to only increase by 6% ± 3% (i.e. mean ± standard deviation among simulations driven by the three CMIP5 ESMs) under the RCP4.5 and nearly zero-change with a large among-model variation (0.3% ± 5%) under the RCP8.5 scenarios (Fig. 3a). However, the MARB annual N loading would increase by ~30% during the last three decades of the 21st century under the RCP4.5 (30% ± 3%) and the RCP8.5 (31% ± 14%) scenarios, compared to the most recent three decades (Fig. 3b). All other input drivers being equal, model simulations indicate that the estimated discharge and N loading show a larger uncertainty under the RCP8.5 scenario than the RCP4.5 scenario (Fig. 3a,b), corresponding to the divergence among future climate projections. Using projected climate from six CMIP5 ESMs under the RCP8.5 scenario, Kujawa et al., (2020) demonstrated that variation among climate models was the dominant source of uncertainty in predicting future total discharge and total N loading in a watershed located in northwest Ohio. This study supports our findings regarding uncertainty sources in projected discharge and N loading in the MARB.

To gain insights into the impacts of future precipitation changes on N export, we quantify the contributions of HP events, non-HP events, and no-precipitation days to water yield (i.e., the sum of surface runoff and drainage runoff) and N yield (i.e., N leaching from soils) across the MARB. Under the RCP4.5 scenario, HP-induced water yield change (49.1±16.8 km^3 yr^{-1}) would dominate the total water yield increase (44.8±20.3 km^3 yr^{-1}) (Fig. 3c and Table S3). For the

RCP8.5 scenario, while the water yield increase on the HP days is more robust (64.1±16.4 km^3 yr^{-1}), it is offset by the decreases in water yield during non-HP days (-35.5±19.9 km^3 yr^{-1}) and no-precipitation days (-25.3±18 km^3 yr^{-1}). The offset of daily water yield leads to a small net increase in the annual total water yield (3.3±32.6 km^3 yr^{-1}) under the RCP8.5 scenario, despite a large among-model variation (Fig. 3c and Table S3).

Along with the total water yield increase, the projected change in total N yield would increase up to 0.55 (± 0.11) Tg yr^{-1} for the RCP4.5 scenario (Fig. 3d). Surprisingly, despite the small increase in total water yield, the projected total N yield would increase by 0.68 (± 0.33) Tg yr^{-1} under the RCP8.5 scenario (Fig. 3d). Specifically, we find that the increases in HP amount would on average account for 45% (0.25±0.05 Tg yr^{-1}) and 56% (0.38±0.18 Tg yr^{-1}) of the total N yield increase under the RCP4.5 and the RCP8.5 scenarios, respectively (Fig. 3d and Table S4). With the changes in the HP-induced water yield (Fig. 3c), our modeling results highlight the significant roles of future HP in contributing N yield across the MARB (Fig. 3d). The results for the RCP8.5 scenario indicate that the riverine N concentration would increase, which likely drives the further deterioration of water quality in the region (Davidson et al., 2011).

Furthermore, the projected changes of N yield also highlight the critical role of days without precipitation in flushing out N, particularly under the RCP8.5 scenario (Fig. 3d). Specifically, the N yield from only drainage runoff (i.e. baseflow) occurring on no-precipitation days would account for 39% (0.21±0.07 Tg yr^{-1}) and 37% (0.25±0.15 Tg yr^{-1}) of the total N yield increase under the RCP4.5 and RCP8.5 scenarios, respectively (Fig. 3d and Table S4). These findings indicate the significant legacy effects after rainfall events on N yield under future climate scenarios.

Compared with HP and no-precipitation events, the small increases in non-HP frequency and intensity (Table S4) would accordingly play a smaller role in determining N yield, only accounting for 16% (0.09±0.02 Tg yr^{-1}) and 8% ± (0.05±0.02 Tg yr^{-1}) of total N yield increases under the RCP4.5 and RCP8.5 scenarios, respectively (Fig. 3d and Table S4). This is likely due to longer drought periods and the decreases in the number of non-HP events by the end of the century (Fig. S7). It is also noteworthy that our predictions have large among-model variations, especially for the RCP8.5 scenario (Fig. 3).

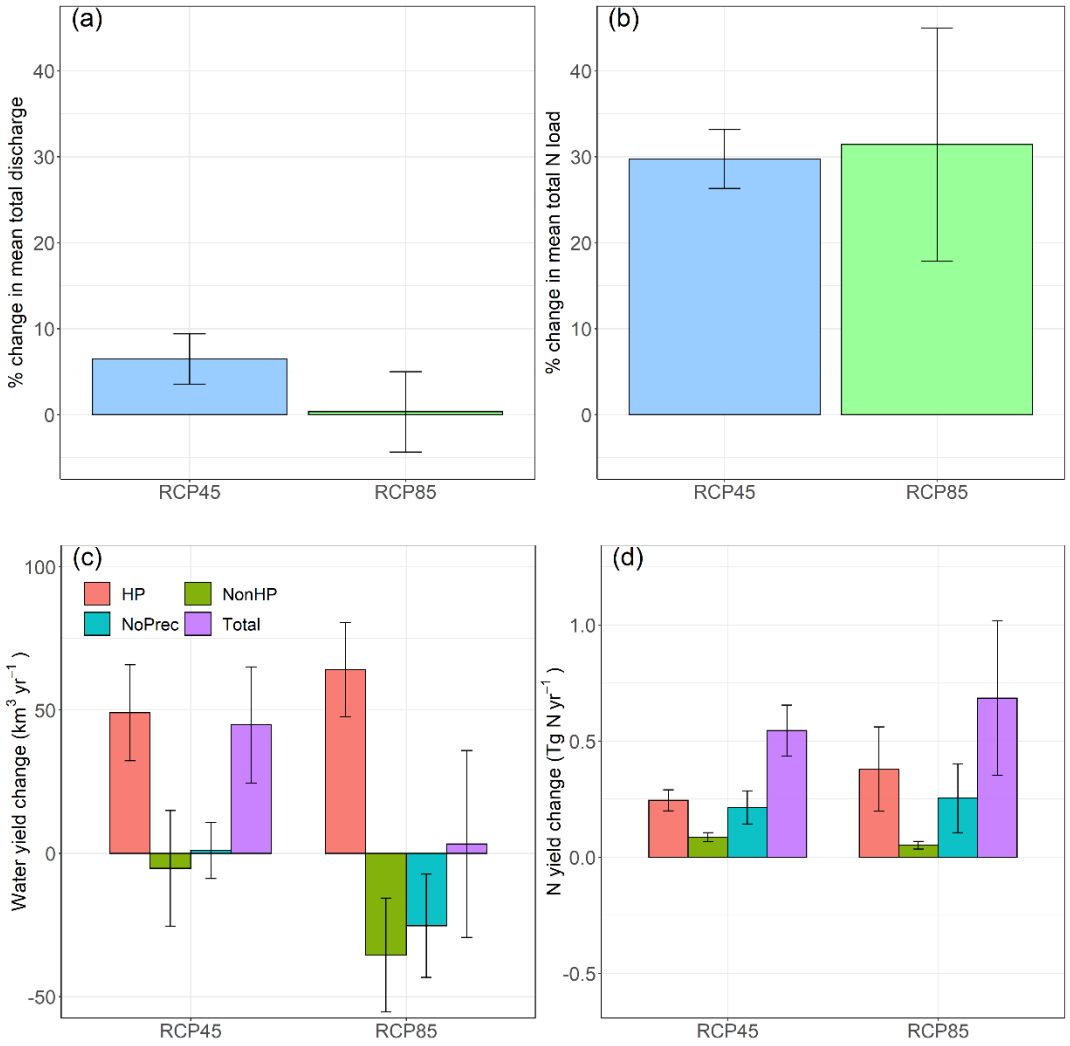

Figure 3. Predicted changes in annual river discharge, N loading, water yield (i.e., the sum of surface and sub-surface runoff), and N yield (i.e., N leaching from soils, calculated as a sum of all simulation grids) from the MARB at the end of the century under the RCP4.5 and RCP8.5 scenarios. **a**,**b**, the change of annual total river discharge (**a**) and annual total N loading (**b**) is calculated as the difference between the period of 2070-2099 and the period of 1988-2017 under the RCP4.5 and RCP8.5 scenarios. **c**,**d**, the change of water yield (**c**) and N yield (**d**) occurred in HP days, non-HP days, and no-precipitation days is calculated as the difference between the period of 2070-2099 and the period of 1988-2017 under the two climate scenarios. The error bars are the standard deviation among DLEM model simulations driven by climate scenario data from three CMIP5 models.

The seasonality of N fluxes in the MARB promotes the development of extensive seasonal hypoxia in the Gulf of Mexico (Donner & Kucharik, 2008) and has important implications for upstream agricultural management selection and planning (e.g., fertilizer application) (Wine et al., 2020). We quantified seasonal changes in N loading from the Basin. About 41% and 51% (i.e., 0.12 and 0.15 Tg N season^{-1}) of the annual N loading increase would come from spring under the RCP4.5 and Rcp8.5 scenarios, respectively (Fig. 4). In the presence of recurrent anthropogenic N fertilizer input across the MARB, increases in spring precipitation (Fig. S8a) would cause higher N yield from land (Fig. S8b). It is noteworthy that the increase in HP-induced N yield accounts for 51% (RCP4.5) and 63% (RCP8.5) of the annual total N yield increase (Fig. S8b), which is likely the major driver for the N loading increase in spring. The increase in N loading over the summer months would be ~26% (i.e., ~0.08 Tg season^{-1}) of the annual N loading increase under both RCP scenarios, which is mainly driven by non-heavy precipitation (Fig. S8). Although lower future N loading increases tend to occur in fall and

417 winter (Fig. 4), they would be driven by increases in HP during low discharge periods (Fig. S8).
418 Model simulations present that the estimated seasonal changes in N loading have a larger
419 uncertainty under both RCP scenarios, especially in spring, which is due to the divergence
420 among future climate projections.

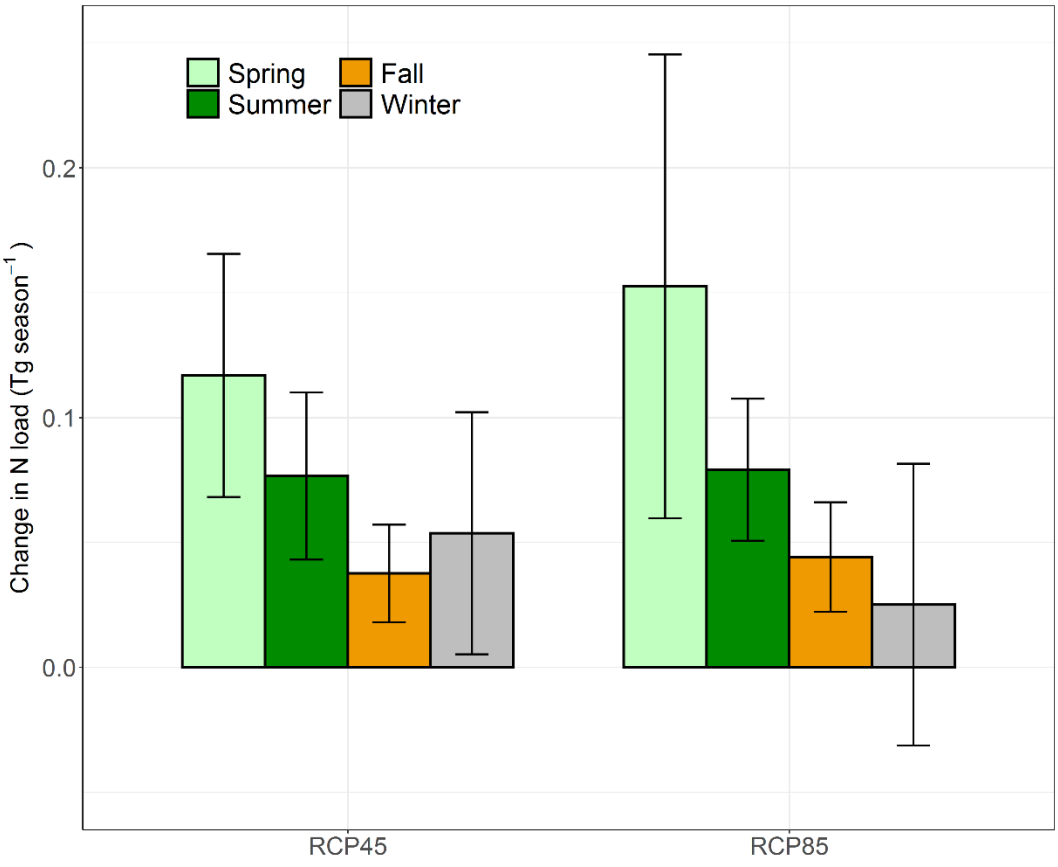

421

422 Figure 4. Predicted changes in seasonal total N loading from the MARB at the end of the century
423 under the RCP4.5 and RCP8.5 scenarios. The change of N loading indicates how far the
424 predicted N loadings during 2070-2099 under the RCP4.5 and the RCP8.5 scenarios are away
425 from the historical model-estimated N loading during 1988-2017. Spring: March, April, and May
426 (MAM); Summer: June, July, and August (JJA); Fall: September, October, and November
427 (SON); Winter: December, January, and February (DJF). The error bars are the standard

deviation of DLEM-estimated N loading changes driven by climate scenario data from three CMIP5 models.

3.3 Spatial Patterns of Water Yield and Nitrogen Yield across the MARB

Widespread increases in total water yield by the end of the century are predicted across the MARB under the two future scenarios (Fig. 5a,b). The predicted increases in total N yield in the upper- and mid-Mississippi River Basins stand out under both RCP scenarios (Fig. 5e,f) despite the predicted increases of annual aridity (Fig. S7). These regions are the home to more than half of the U.S. agricultural production (Yu & Lu, 2018), where more N fertilizer is applied than anywhere else in the U.S. (Cao et al., 2018; Lu et al., 2019; Zhang, Cao, et al., 2021). Specifically, the water yield increases on the HP days under the RCP8.5 scenario would be more spatially extended than those under the RCP4.5 scenario (Fig. 5c,d), leading to an overall higher N yield (Fig. 5g,h), especially in the upper-Mississippi River Basin. The Mississippi Alluvial Plain (referring to the region with the highest rice production in the southern four states, including Arkansas, Louisiana, Mississippi, and Texas, in the U.S.) in the southern MARB also displays significant increases in N yield when HP events would occur in the future (Fig. 5c,d).

We also find that water yield on the non-HP days would decline over a large portion of the MARB, while the declines in N yield would not be as widespread as water yield (Figs. S9a,b and S10a,b). It is noteworthy that, on no-precipitation days, the areas with declined water yield would be mainly located in the southern and western MARB and would be larger than the areas with increases in water yield (Fig. S9c,d). These water yield changes over space lead to a basin-wide negligible change and a slight decrease in water yield under the RCP4.5 and the RCP8.5 scenarios, respectively (Fig. 5c). However, increased water yield (Fig. S9c,d), continued intensive fertilizer use, and a greater preponderance of tile drainage in the agriculture-dominated

451 watersheds in the Midwest would together drive robust N yield during the no-precipitation days
452 for the two RCP scenarios (Figs. S10c,d). These hotspots indicate the potential legacy effects
453 after rainfall events on N yield, depending on the regions and N input amount applied to the
454 cropland surface (Van Meter et al., 2016, 2017, 2018).

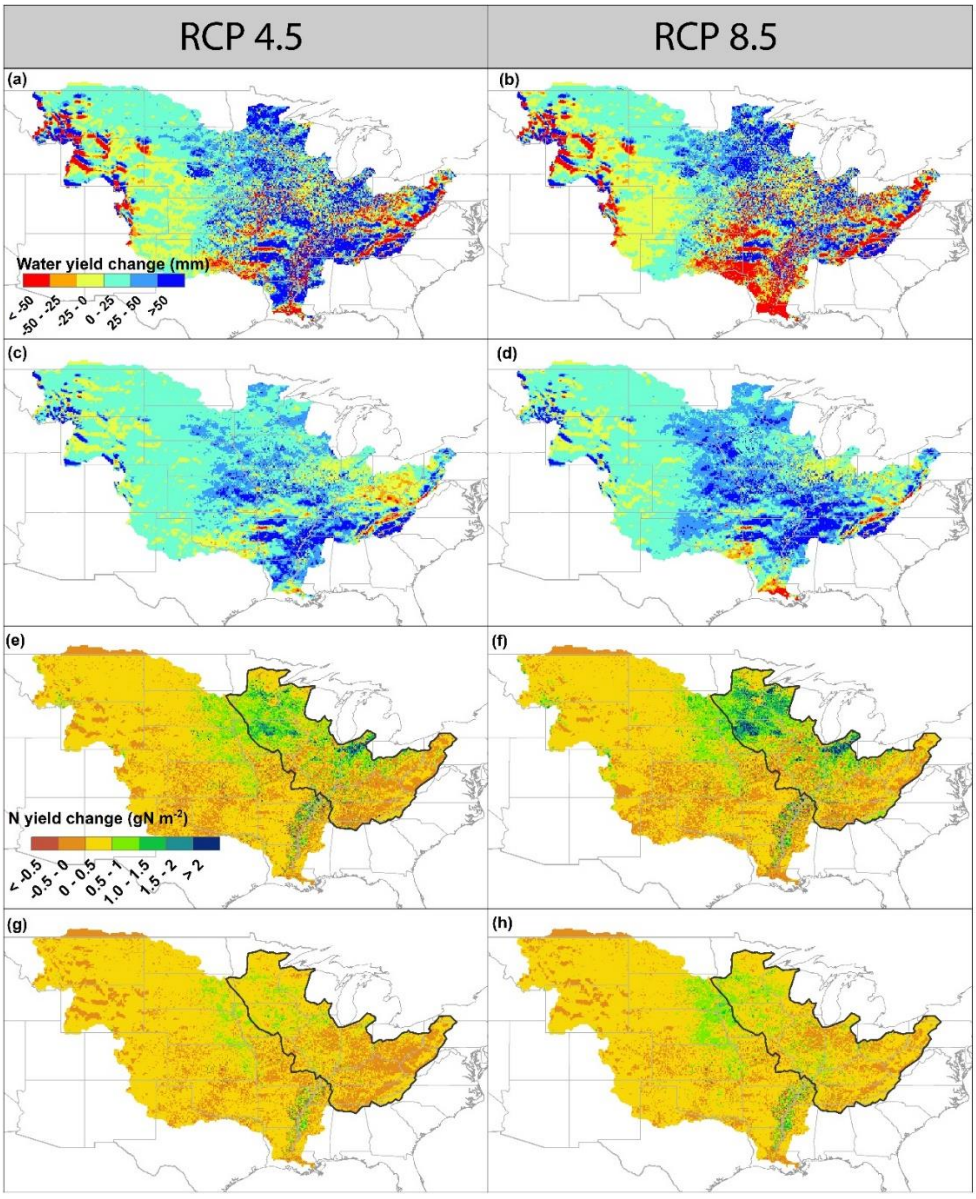

455

456 Figure 5. Predicted changes in total water yield and total N yield at the end of the century. The
457 predicted changes in annual total water yield (a and b) and HP-day water yield (c and d) between

458 the period of 2070-2099 and the period of 1988-2017 under the RCP4.5 (**a, c**) and RCP8.5 (**b, d**)
459 scenarios. The predicted change in annual total N yield (e and f) and HP-day N yield (g and h)
460 between the period of 2070-2099 and the period of 1988-2017 under the RCP4.5 (**e, g**) and
461 RCP8.5 (**f, h**) scenarios. The black outlines in sub-figures **e-h** highlight the upper-, mid-
462 Mississippi River Basins, and the Ohio River Basin.

463 **3.4 Spatial Variations of Water Yield and Nitrogen Yield**

464 Our results indicate that future climate conditions associated with the high-emission scenario
465 would bring a bigger challenge for the stakeholders to reduce N leaching in the MARB. This
466 conclusion is supported by a recent study (Sinha et al., 2017), which focuses on exploring the
467 annual and seasonal patterns of precipitation in determining N load. Divergences in precipitation
468 projections among CMIP5 models translate into large variations in the magnitude of predicted
469 water and N yield changes across the MARB (Figs. S11-S13), illustrating the importance of
470 reducing uncertainties in the future climate projections (Sinha et al., 2017). For water yield
471 induced by HP events, the central and southeastern MARB display the largest among-model
472 variations (e.g., up to 110 mm yr^{-1} and 120 mm yr^{-1} under the RCP4.5 and RCP8.5 scenarios,
473 respectively) (Fig. S11a,b). Large variations in N yield are also found in both the Corn Belt and
474 the Mississippi Alluvial Plain under future scenarios (Fig. S11c,d). Specifically, the highest N
475 yield variation would likely occur in the Mississippi Alluvial Plain, which would reach up to 0.8
476 g N m^{-2} yr^{-1} and 2.4 g N m^{-2} yr^{-1} under the RCP4.5 and the RCP8.5 scenarios, respectively.
477 Compared with the RCP4.5 scenario, a larger spatial extent of N yield variation is found under
478 the RCP8.5 scenario. These spatial patterns of N yield variations highlight the challenges to
479 implementing region-specific N mitigation practices in watersheds with high N inputs and more
480 frequent and extreme precipitation (Fig. S12). Also, future studies should pay more attention to

481 the uncertainties in predicting HP-induced water yield and N yield using climate models from the
482 CMIP5 ensemble.

483 Compared with the HP days, the among-model variations in water yield (e.g., <40mm yr^{-1})
484 and N yield (e.g., <0.6 g N m^{-2} yr^{-1}) during the non-HP days present lower magnitude and
485 smaller extent across the Basin (Figs. S12 and S13). This implies that the non-HP predictions are
486 relatively convergent among the three CMIP5 models, and so are their impacts on future water
487 and N yields. Although the spatial extent of water and N yield variations under no-precipitation
488 days are smaller than those under the HP days, higher variation magnitudes (e.g., >40mm yr^{-1} for
489 water yield; >0.6 g N m^{-2} yr^{-1} for N yield) are detected in the Midwestern states like Iowa and
490 Indiana (Fig. S13). Between the two RCP scenarios, the water yield and N yield during the non-
491 HP days and no-precipitation days would be more variable under the RCP8.5 scenario. These
492 spatial variations suggest that heavy precipitation would play a significant role in determining
493 future water and N yields. However, the climate models contain large uncertainties in predicting
494 the occurrence and severity of heavy rainfall events.

495 **4. Uncertainties and Limitations**

496 Our study involves uncertainties in the following aspects. First, uncertainties existing in the 21st-
497 century CMIP5 precipitation projections dominate the uncertainties of predicted water and N
498 yields across the MARB. These sources of CMIP5 projection uncertainty are generally classified
499 into three types: internal variability, inter-model variability, and greenhouse gas emissions (Chen
500 et al., 2014). Kharin et al., (2013) showed that confidence in the projected changes in extreme
501 precipitation is low in the tropics due to the large inter-model disagreements, indicating that
502 some physical processes associated with extreme precipitation may not be well represented in the
503 current generation of models. Our uncertainty analyses of changes in future HP, water yield, and

N yield also demonstrate a relatively high inter-model disagreement in the southern parts of the Basin (Figs. S5c,d and S11-S13). Using CMIP5 models, Chen et al., (2014) found that internal and inter-model variability are the dominant sources of uncertainty in global precipitation-related extremes. However, the increases in intensified extreme precipitation occurring in North America detected in the CMIP5 models demonstrate a higher inter-model agreement than other regions around the globe (Chen et al., 2014). Therefore, the uncertainties of modeled water and N yields across the MARB presented in our study are highly driven by uncertainties in future climate projections, particularly for the HP events. Systematic analyses of N load uncertainty sources deserve further research efforts.

Second, our analyses only considered the same-day HP-induced water and N yields. Soil water content can be largely increased by extreme rainfall events and persists over the following days, leading to a consistently high baseflow and consequently high N leaching for several days. In our analysis, however, we classified the N yield following the HP events into the N yield occurring on no-precipitation days. This assumption potentially underestimates the "HP-induced" N yield and load but overestimates those occurring on no-precipitation days. Therefore, our modeled N loads can be treated as a lower limit of the real-world N loads induced by HP events. Based on our conservative modeling estimates, we can foresee that the extreme N loads and eutrophication peaks in the Gulf would likely be larger after future extreme precipitation events. Effects on water quality of extreme precipitation, and of its legacy, merit further analysis.

Third, N fertilizer input data used by our model relies on the state-level crop-specific N fertilizer use survey, assuming N fertilizer applied to the same crops is at a uniform rate within a state. Due to limited information, we multiplied the N fertilizer use rate by the state-level crop-specific fertilized area percentage (e.g., 98% of corn is fertilized and 2% is non-fertilized in Iowa,

Lu et al., (2019)). This step "dilutes" the fertilizer input while guaranteeing the total N fertilizer amount is consistent with the state-level survey data. Nevertheless, the consequence of this modification leads to a case that the areas without N fertilization would also receive the same state-level N input rate as other fertilized areas in that state. Although the unfertilized area is very low for most crops, the spatial extent of N yield and loading estimated in our study would likely be overestimated across the Basin while the magnitude is underestimated in fertilized soils. Crop-specific N fertilizer use rates at a finer spatial scale (e.g., county-level) can be essential for improving the prediction accuracy of excess N load in a changing climate.

5. Recommendations for Future N Management in the MARB

Concentrated precipitation bursts with durations of a few hours are projected to be more common (Westra et al., 2013). Increases in extreme precipitation are likely to be accompanied by increases in extreme nutrient loading (Carpenter et al., 2018). As Fig. 6 demonstrates, our modeling results suggest that precipitation changes in agricultural regions would likely intensify N pollution in the Gulf of Mexico by the end of the century. As temperature increases (Fig. 1a) and precipitation becomes more variable and extreme (Fig. 1b and S5), droughts would become more common under the RCP8.5 scenario (Fig. S7), which can intensify N loading and its variation (Fig. 6). Drought decreases N loading due to short-term low water flows. However, rapid transitions from dry to wet conditions lead to increased N fluxes (Loecke et al., 2017). Inorganic N that is easily mobilized may accumulate in the soil during drought periods. Subsequent heavy or non-heavy rainfall events could exacerbate N leaching by flushing out the unused residual soil N (Lee et al., 2016; Morecroft et al., 2000; Shepherd et al., 2018; Zhang, Lu, et al., 2021).

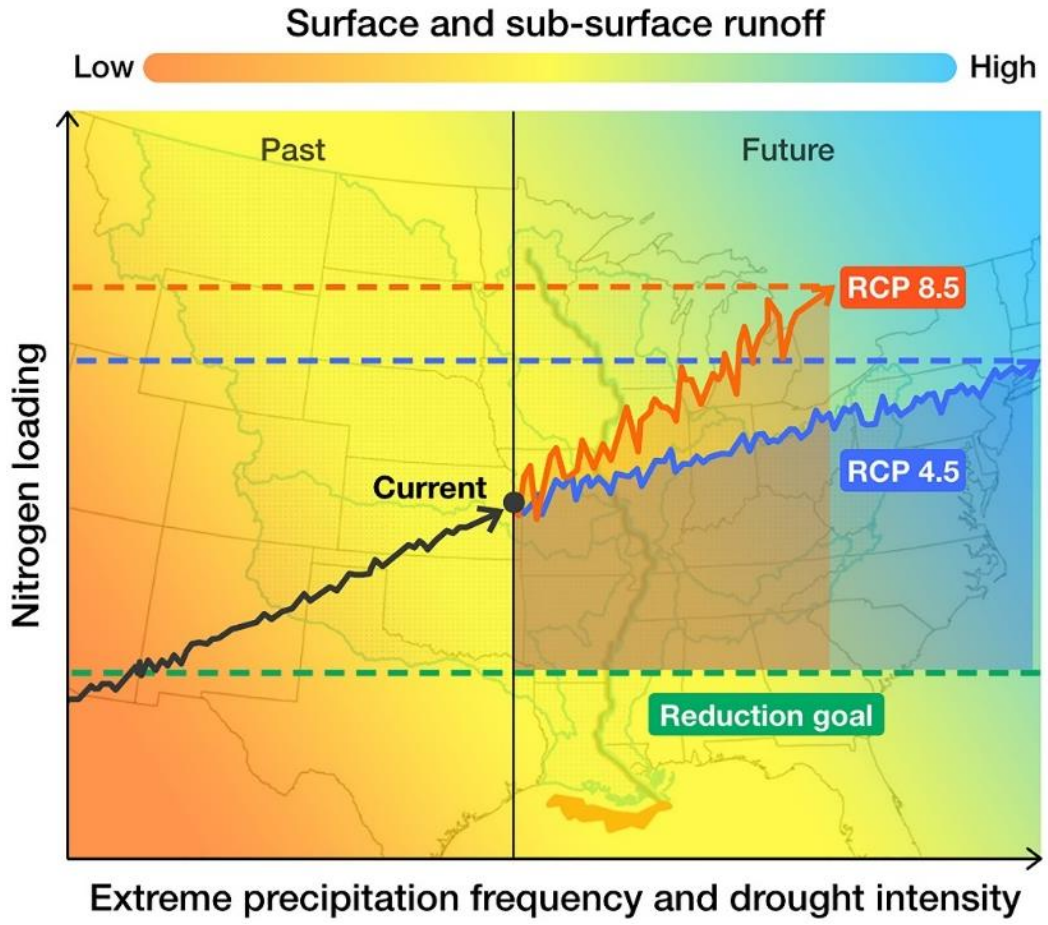

Figure 6. Conceptual diagram of possible trajectories of nitrogen (N) loading changes induced by heavy rainfall intensity and frequency under future climate and management scenarios. The trajectory of N loading illustrated in this figure is not a reflection of the real-world annual total N loading trend in the MARB but is used to represent the potential "cause-effect" between N loading and increases in heavy rainfall frequency and intensity in the Basin. As indicated by this study, the RCP8.5 scenario is likely to yield a smaller increase of runoff but a larger N loading than the RCP4.5 scenario under the same level of anthropogenic N input.

It is also important to emphasize that the current agricultural production systems would likely adapt to the changes in total precipitation, heavy precipitation, and seasonal patterns. Much of the Corn Belt region receives more-than-adequate precipitation during the growing season, and

560 the landscape has been hydrologically altered to hasten the transfer of water to the stream
561 network (Dai et al., 2016; Kelly et al., 2017; Munoz et al., 2018) to maximize crop production.
562 These alterations, which include stream straightening, ditch construction, drainage of wetlands,
563 and lowering the water table using subsurface networks of porous pipes, have magnified
564 agricultural N loss and downstream eutrophication (Skaggs et al., 1994). DIN loading in May is
565 the best predictor of the areal extent of summer hypoxia in the Gulf of Mexico (Turner et al.,
566 2006). As heavy precipitation would increase in spring (Fig. S8a), Corn Belt farmers are likely to
567 intensify their drainage practices (Singh et al., 2009) and increase N inputs (Houser et al., 2019)
568 while attempting to maintain production levels, multiplying the effects of climate change alone
569 on N loads and hypoxia in summer. Particularly in the Midwest, the majority of N fertilizer is
570 applied before crops are planted. For example, corn N fertilizer application before crop planting
571 (in spring only) accounts for 43% of annual N fertilizer usage in Iowa and 59% in Minnesota,
572 and the amounts of N fertilizer applied at crop planting (9% in Iowa and 5% in Minnesota), after
573 crop planting (25% and 4%), and after crop harvest (in the fall of the previous year, 23% and
574 32%) are all less than that applied in spring before crop planting (Cao et al., 2018). With the
575 current N input strategy, increases in heavy precipitation are likely to cause increases in N
576 loading, especially in spring when before-planting and at-planting N fertilizer are applied (Fig. 4
577 and Fig. S8). We found that more than one third of the annual total HP-induced N yield across
578 the basin would be from spring (37% under the RCP4.5 and 40% under the RCP8.5 scenarios).
579 Hence land managers should adopt more aggressive management intervention and advanced
580 technologies, such as monitoring crop N demands for precision fertilizer use, using slow-
581 releasing fertilizer type, to reduce the adverse impacts of heavy precipitation events while
582 maintaining crop production. Additionally, side-dressing and postponing fall as well as spring

583 before-planting fertilizer application until crop germinates could be effective to lessen the risk of
584 N loss under heavy rainfall events (Lu et al., 2020). Nevertheless, an existing study argued that
585 the CMIP5 climate models tend to overestimate the number of spring extreme precipitation
586 events and underestimate summer events in the contiguous United States compared to
587 observations (e.g., summer events were underestimated by 16% and spring events overestimated
588 by 14% in the Midwestern U.S.) (Janssen et al., 2016). This might slightly contribute to the large
589 spring increases in the N yield and loading estimated in our study. The effects of climate and
590 land management on nutrient export from agricultural systems remain as the current research
591 challenge that involves multiple climatic variables, landscape heterogeneity, and agricultural
592 practices (Deshmukh & Singh, 2016; Frans et al., 2013; Gupta et al., 2015; Martin et al., 2017;
593 Shang, 2019). More research is needed to clarify the roles of heavy precipitation changes vs.
594 agricultural management (e.g., rotation, tile drainage, N fertilizer application timing, etc.) for
595 nutrient loading. To reach the reduction goals of N load and hypoxia in the Gulf of Mexico, we
596 need to take the trajectories of future extreme climate into account to assess and improve the
597 mitigation efforts.

598 Our conclusions drawn here have global implications for watershed nutrient management and
599 eutrophication reduction in the coasts given the future changing climate and enhanced
600 hydroclimatic extreme events. Our recent analyses revealed that extreme precipitation events
601 have been expanding to states in the upper-Mississippi River Basin where N fertilizers are used
602 more intensively (Lu et al., 2020). Understanding the extreme climate trends could inform farm-
603 management practices and lessen the likelihood of N loading in waterways. For example, land
604 managers may use cover crops to enhance long-term ecosystem N retention capability, reduce N
605 input amount using rotation system, and modify fertilizer application timing to meet crop

606 nutrient demands while minimizing the contribution of extreme precipitation events. We have
607 demonstrated that historical N loading from the MARB to the Gulf of Mexico could be reduced
608 by up to 16% if N fertilizers are applied multiple times after crops develop, without affecting
609 crop productivity, when there is less likelihood of heavy precipitation events (Lu et al., 2020). To
610 achieve the feasibility of water pollution mitigation, we appeal that more studies are needed to
611 interpret the relative effects of extreme climate and land management practices, such as cover
612 crops, riparian buffers, side-dressed N fertilizer, precision N management and so on, on N
613 outputs from agricultural watersheds.

614 **Data availability**

615 The data supporting the major findings of this study, including annual average climate conditions
616 as well as the statistics of model-estimated river discharge, N load, water and N yield across the
617 Basin, can be found in https://doi.org/10.6084/m9.figshare.19394132.v1. The raw model outputs
618 from this study are accessible upon request (contact: clu@iastate.edu).

619 **Acknowledgments**

620 This work is supported partially by Iowa Nutrient Research Center, the NSF grant (1903722), the
621 NSF CAREER (1945036), and ISU postdoc seed grant. We thank the two anonymous reviewers
622 for improving the manuscript.

623 **Author contributions**

624 J.Z. and C.L. conceived and designed the research, analyzed the model results, and wrote the
625 manuscript. J.Z. collected data, calibrated and validated the model, and carried out modeling
626 experiments. W.C., C.J., H.T., G.V., K.S., and D.G. helped with data interpretation and
627 discussion. All co-authors reviewed and contributed to the manuscript.

Additional information

Correspondence and requests for materials should be addressed to C.L.

Competing interests

The authors declare no competing interests.

References

Abatzoglou, J. T. (2013). Development of gridded surface meteorological data for ecological applications and modelling. *International Journal of Climatology*, *33*(1), 121–131.

Abatzoglou, J. T., & Brown, T. J. (2012). A comparison of statistical downscaling methods suited for wildfire applications. *International Journal of Climatology*, *32*(5), 772–780.

Aulenbach, B. T., Buxton, H. T., Battaglin, W. A., & Coupe, R. H. (2007). *Streamflow and nutrient fluxes of the Mississippi-Atchafalaya River Basin and subbasins for the period of record through 2005*. US Geological Survey.

Ballard, T. C., Sinha, E., & Michalak, A. M. (2019). Long-term changes in precipitation and temperature have already impacted nitrogen loading. *Environmental Science & Technology*, *53*(9), 5080–5090.

Cao, P., Lu, C., & Yu, Z. (2018). Historical Nitrogen Fertilizer Use in Agricultural Ecosystems of The Contiguous United States during 1850–2015: Application Rate, Timing, and Fertilizer Types. *Earth System Science Data*, *10*(2), 969–984.

Carpenter, S. R., Booth, E. G., & Kucharik, C. J. (2018). Extreme precipitation and phosphorus loads from two agricultural watersheds. *Limnology and Oceanography*, *63*(3), 1221–1233.

Chen, H., Sun, J., & Chen, X. (2014). Projection and uncertainty analysis of global precipitation-related extremes using CMIP5 models. *International Journal of Climatology*, *34*(8), 2730–2748.

Clarke, L., Edmonds, J., Jacoby, H., Pitcher, H., Reilly, J., & Richels, R. (2007). Scenarios of greenhouse gas emissions and atmospheric concentrations.

Collins, W. J., Bellouin, N., Doutriaux-Boucher, M., Gedney, N., Halloran, P., Hinton, T., et al. (2011). Development and evaluation of an Earth-System model–HadGEM2. *Geosci. Model Dev. Discuss*, *4*(2), 997–1062.

Dai, S., Shulski, M. D., Hubbard, K. G., & Takle, E. S. (2016). A spatiotemporal analysis of Midwest US temperature and precipitation trends during the growing season from 1980 to 2013. *International Journal of Climatology*, *36*(1), 517–525.

Davidson, E. A., David, M. B., Galloway, J. N., Goodale, C. L., Haeuber, R., Harrison, J. A., et al. (2011). Excess nitrogen in the US environment: trends, risks, and solutions. *Issues in Ecology*, (15).

662 Dentener, F. J. (2006). Global Maps of Atmospheric Nitrogen Deposition, 1860, 1993, and 2050.
663 https://doi.org/10.1016/j.ridd.2011.06.019

664 Deshmukh, A., & Singh, R. (2016). Physio-climatic controls on vulnerability of watersheds to
665 climate and land use change across the US. *Water Resources Research*, *52*(11), 8775–8793.

666 Donner, S. D., & Kucharik, C. J. (2003). Evaluating the impacts of land management and climate
667 variability on crop production and nitrate export across the Upper Mississippi Basin. *Global*
668 *Biogeochemical Cycles*, *17*(3).

669 Donner, S. D., & Kucharik, C. J. (2008). Corn-based ethanol production compromises goal of
670 reducing nitrogen export by the Mississippi River. *Proceedings of the National Academy of*
671 *Sciences*, *105*(11), 4513–4518.

672 Dunne, J. P., John, J. G., Shevliakova, E., Stouffer, R. J., Krasting, J. P., Malyshev, S. L., et al.
673 (2013). GFDL's ESM2 global coupled climate–carbon earth system models. Part II: carbon
674 system formulation and baseline simulation characteristics. *Journal of Climate*, *26*(7),
675 2247–2267.

676 Evans, A. E. V, Hanjra, M. A., Jiang, Y., Qadir, M., & Drechsel, P. (2012). Water quality:
677 assessment of the current situation in Asia. *International Journal of Water Resources*
678 *Development*, *28*(2), 195–216.

679 Frans, C., Istanbulluoglu, E., Mishra, V., Munoz-Arriola, F., & Lettenmaier, D. P. (2013). Are
680 climatic or land cover changes the dominant cause of runoff trends in the Upper Mississippi
681 River Basin? *Geophysical Research Letters*, *40*(6), 1104–1110.

682 Grizzetti, B., Bouraoui, F., Billen, G., van Grinsven, H., Cardoso, A. C., Thieu, V., et al. (2011).
683 Nitrogen as a threat to European water quality.

684 Gupta, S. C., Kessler, A. C., Brown, M. K., & Zvomuya, F. (2015). Climate and agricultural land
685 use change impacts on streamflow in the upper midwestern United States. *Water Resources*
686 *Research*, *51*(7), 5301–5317.

687 Houser, M., Gunderson, R., & Stuart, D. (2019). Farmers' Perceptions of Climate Change in
688 Context: Toward a Political Economy of Relevance. *Sociologia Ruralis*, *59*(4), 789–809.

689 Howarth, R. W., & Marino, R. (2006). Nitrogen as the limiting nutrient for eutrophication in
690 coastal marine ecosystems: evolving views over three decades. *Limnology and*
691 *Oceanography*, *51*(1part2), 364–376.

692 Howarth, R. W., Anderson, D., Cloern, J., Elfring, C., Hopkinson, C., Lapointe, B., et al. (2000).
693 Nutrient pollution of coastal rivers, bays, and seas. *Issues in Ecology*, *7*, 1–15. Retrieved
694 from http://pubs.er.usgs.gov/publication/70185674

695 Howarth, R. W., Swaney, D. P., Boyer, E. W., Marino, R., Jaworski, N., & Goodale, C. (2006).
696 The influence of climate on average nitrogen export from large watersheds in the
697 Northeastern United States. In *Nitrogen Cycling in the Americas: Natural and*
698 *Anthropogenic Influences and Controls* (pp. 163–186). Springer.

699 Janssen, E., Sriver, R. L., Wuebbles, D. J., & Kunkel, K. E. (2016). Seasonal and regional
700 variations in extreme precipitation event frequency using CMIP5. *Geophysical Research*

Letters, *43*(10), 5385–5393.

Kelly, S. A., Takbiri, Z., Belmont, P., & Foufoula-Georgiou, E. (2017). Human amplified changes in precipitation-runoff patterns in large river basins of the Midwestern United States. *Hydrology and Earth System Sciences*, *21*(10), 5065–5088. https://doi.org/10.5194/hess-21-5065-2017

Kharin, V. V, Zwiers, F. W., Zhang, X., & Wehner, M. (2013). Changes in temperature and precipitation extremes in the CMIP5 ensemble. *Climatic Change*, *119*(2), 345–357.

Kujawa, H., Kalcic, M., Martin, J., Aloysius, N., Apostel, A., Kast, J., et al. (2020). The hydrologic model as a source of nutrient loading uncertainty in a future climate. *Science of The Total Environment*, *724*, 138004.

Lee, M., Shevliakova, E., Malyshev, S., Milly, P. C. D., & Jaffé, P. R. (2016). Climate variability and extremes, interacting with nitrogen storage, amplify eutrophication risk. *Geophysical Research Letters*. https://doi.org/10.1002/2016GL069254

Liu, M., Tian, H., Yang, Q., Yang, J., Song, X., Lohrenz, S. E., & Cai, W. J. (2013). Long-term trends in evapotranspiration and runoff over the drainage basins of the Gulf of Mexico during 1901-2008. *Water Resources Research*, *49*(4), 1988–2012. https://doi.org/10.1002/wrcr.20180

Loecke, T. D., Burgin, A. J., Riveros-Iregui, D. A., Ward, A. S., Thomas, S. A., Davis, C. A., & Clair, M. A. S. (2017). Weather whiplash in agricultural regions drives deterioration of water quality. *Biogeochemistry*, *133*(1), 7–15.

Lu, C., & Tian, H. (2017). Global nitrogen and phosphorus fertilizer use for agriculture production in the past half century: shifted hot spots and nutrient imbalance. *Earth System Science Data*, *9*(1), 181–192.

Lu, C., Yu, Z., Tian, H., Hennessy, D. A., Feng, H., Al-Kaisi, M., et al. (2018). Increasing carbon footprint of grain crop production in the US Western Corn Belt. *Environmental Research Letters*, *13*(12), 124007.

Lu, C., Zhang, J., Cao, P., & Hatfield, J. (2019). Are We Getting Better in Using Nitrogen?: Variations in Nitrogen Use Efficiency of Two Cereal Crops Across the United States. *Earth's Future*, *7*(8), 939–952. https://doi.org/10.1029/2019EF001155

Lu, C., Zhang, J., Tian, H., Crumpton, W. G., Helmers, M. J., Cai, W.-J., et al. (2020). Increased extreme precipitation challenges nitrogen load management to the Gulf of Mexico. *Communications Earth & Environment*, *1*(1), 21. https://doi.org/10.1038/s43247-020-00020-7

Malone, R. W., Kersebaum, K. C., Kaspar, T. C., Ma, L., Jaynes, D. B., & Gillette, K. (2017). Winter rye as a cover crop reduces nitrate loss to subsurface drainage as simulated by HERMES. *Agricultural Water Management*, *184*, 156–169.

Mananze, S., Pôças, I., & Cunha, M. (2019). Agricultural drought monitoring based on soil moisture derived from the optical trapezoid model in Mozambique. *Journal of Applied Remote Sensing*, *13*(2), 24519.

740 Martin, K. L., Hwang, T., Vose, J. M., Coulston, J. W., Wear, D. N., Miles, B., & Band, L. E.
741 (2017). Watershed impacts of climate and land use changes depend on magnitude and land
742 use context. *Ecohydrology*, *10*(7), e1870.

743 Mesinger, F., DiMego, G., Kalnay, E., Mitchell, K., Shafran, P. C., Ebisuzaki, W., et al. (2006).
744 North American regional reanalysis. *Bulletin of the American Meteorological Society*, *87*(3),
745 343–360.

746 Van Meter, K. J., Basu, N. B., Veenstra, J. J., & Burras, C. L. (2016). The nitrogen legacy:
747 Emerging evidence of nitrogen accumulation in anthropogenic landscapes. *Environmental*
748 *Research Letters*. https://doi.org/10.1088/1748-9326/11/3/035014

749 Van Meter, K. J., Basu, N. B., & Van Cappellen, P. (2017). Two centuries of nitrogen dynamics:
750 Legacy sources and sinks in the Mississippi and Susquehanna River Basins. *Global*
751 *Biogeochemical Cycles*, *31*(1), 2–23. https://doi.org/10.1002/2016GB005498

752 Van Meter, K. J., Van Cappellen, P., & Basu, N. B. (2018). Legacy nitrogen may prevent
753 achievement of water quality goals in the Gulf of Mexico. *Science*.
754 https://doi.org/10.1126/science.aar4462

755 Mitchell, T. D., & Jones, P. D. (2005). An improved method of constructing a database of
756 monthly climate observations and associated high-resolution grids. *International Journal of*
757 *Climatology*, *25*(6), 693–712. https://doi.org/10.1002/joc.1181

758 Morecroft, M. D., Burt, T. P., Taylor, M. E., & Rowland, A. P. (2000). Effects of the 1995–1997
759 drought on nitrate leaching in lowland England. *Soil Use and Management*, *16*(2), 117–123.

760 Munoz, S. E., Giosan, L., Therrell, M. D., Remo, J. W. F., Shen, Z., Sullivan, R. M., et al. (2018).
761 Climatic control of Mississippi River flood hazard amplified by river engineering. *Nature*,
762 *556*(7699), 95–98.

763 National Academies of Sciences and Medicine, E. (2016). *Attribution of extreme weather events*
764 *in the context of climate change*. National Academies Press.

765 Rabalais, N. N., Turner, R. E., Sen Gupta, B. K., Boesch, D. F., Chapman, P., & Murrell, M. C.
766 (2007). Hypoxia in the northern Gulf of Mexico: Does the science support the plan to
767 reduce, mitigate, and control hypoxia? *Estuaries and Coasts*.
768 https://doi.org/10.1007/BF02841332

769 Riahi, K., Grübler, A., & Nakicenovic, N. (2007). Scenarios of long-term socio-economic and
770 environmental development under climate stabilization. *Technological Forecasting and*
771 *Social Change*, *74*(7), 887–935.

772 Riahi, K., Rao, S., Krey, V., Cho, C., Chirkov, V., Fischer, G., et al. (2011). RCP 8.5—A
773 scenario of comparatively high greenhouse gas emissions. *Climatic Change*, *109*(1), 33–57.

774 Scavia, D., Bertani, I., Obenour, D. R., Turner, R. E., Forrest, D. R., & Katin, A. (2017).
775 Ensemble modeling informs hypoxia management in the northern Gulf of Mexico.
776 *Proceedings of the National Academy of Sciences*. https://doi.org/10.1073/pnas.1705293114

777 Shang, L. (2019). Climate Change And Land Use/cover Change Impacts On Watershed
778 Hydrology, Nutrient Dynamics–A Case Study In Missisquoi River Watershed.

779 Shepherd, M., Lucci, G., Vogeler, I., & Balvert, S. (2018). The effect of drought and nitrogen
780 fertiliser addition on nitrate leaching risk from a pasture soil; an assessment from a field
781 experiment and modelling. *Journal of the Science of Food and Agriculture*, *98*(10), 3795–
782 3805.

783 Singh, R., Helmers, M. J., Kaleita, A. L., & Takle, E. S. (2009). Potential impact of climate
784 change on subsurface drainage in Iowa's subsurface drained landscapes. *Journal of*
785 *Irrigation and Drainage Engineering*, *135*(4), 459–466.

786 Sinha, E., & Michalak, A. M. (2016). Precipitation dominates interannual variability of riverine
787 nitrogen loading across the continental United States. *Environmental Science and*
788 *Technology*. https://doi.org/10.1021/acs.est.6b04455

789 Sinha, E., Michalak, A. M., & Balaji, V. (2017). Eutrophication will increase during the 21st
790 century as a result of precipitation changes. *Science*, *357*(6349), 405–408.

791 Skaggs, R. W., Breve, M. A., & Gilliam, J. W. (1994). Hydrologic and water quality impacts of
792 agricultural drainage∗. *Critical Reviews in Environmental Science and Technology*, *24*(1),
793 1–32.

794 Smith, S. J., & Wigley, T. M. L. (2006). Multi-gas forcing stabilization with Minicam. *The*
795 *Energy Journal*, (Special Issue# 3).

796 Thomas, P., & Rahman, M. S. (2012). Extensive reproductive disruption, ovarian
797 masculinization and aromatase suppression in Atlantic croaker in the northern Gulf of
798 Mexico hypoxic zone. *Proceedings of the Royal Society B: Biological Sciences*, *279*(1726),
799 28–38.

800 Thomson, A. M., Calvin, K. V, Smith, S. J., Kyle, G. P., Volke, A., Patel, P., et al. (2011). RCP4.
801 5: a pathway for stabilization of radiative forcing by 2100. *Climatic Change*, *109*(1), 77–94.

802 Tian, H., Xu, X., Liu, M., Ren, W., Zhang, C., Chen, G., & Lu, C. (2010). Spatial and temporal
803 patterns of CH4 and N2O fluxes in terrestrial ecosystems of North America during 1979–
804 2008: application of a global biogeochemistry model. *Biogeosciences*, *7*(9), 2673–2694.

805 Tian, H., Xu, R., Pan, S., Yao, Y., Bian, Z., Cai, W., et al. (2020). Long-Term Trajectory of
806 Nitrogen Loading and Delivery From Mississippi River Basin to the Gulf of Mexico.
807 *Global Biogeochemical Cycles*, *34*(5), e2019GB006475.

808 Voldoire, A., Sanchez-Gomez, E., y Mélia, D. S., Decharme, B., Cassou, C., Sénési, S., et al.
809 (2013). The CNRM-CM5. 1 global climate model: description and basic evaluation.
810 *Climate Dynamics*, *40*(9–10), 2091–2121.

811 Wei, Y., Liu, S., Huntzinger, D. N., Michalak, A. M., Viovy, N., Post, W. M., et al. (2014). The
812 north american carbon program multi-scale synthesis and terrestrial model intercomparison
813 project - Part 2: Environmental driver data. *Geoscientific Model Development*, *7*(6), 2875–
814 2893. https://doi.org/10.5194/gmd-7-2875-2014

815 Westra, S., Alexander, L. V, & Zwiers, F. W. (2013). Global increasing trends in annual
816 maximum daily precipitation. *Journal of Climate*, *26*(11), 3904–3918.

817 Wine, M. L., Golden, H. E., Christensen, J. R., Lane, C. R., & Makhnin, O. (2020). Seasonal

watershed-scale influences on nitrogen concentrations across the Upper Mississippi River Basin. *Hydrology and Earth System Sciences Discussions*, 1–31.

Wise, M., Calvin, K., Thomson, A., Clarke, L., Bond-Lamberty, B., Sands, R., et al. (2009). Implications of limiting CO2 concentrations for land use and energy. *Science*, *324*(5931), 1183–1186.

Yang, Q., Tian, H., Li, X., Ren, W., Zhang, B., Zhang, X., & Wolf, J. (2016). Spatiotemporal patterns of livestock manure nutrient production in the conterminous United States from 1930 to 2012. *Science of the Total Environment*, *541*, 1592–1602.

Yu, Z., & Lu, C. (2018). Historical cropland expansion and abandonment in the continental US during 1850 to 2016. *Global Ecology and Biogeography*, *27*(3), 322–333.

Yu, Z., Lu, C., Cao, P., & Tian, H. (2018). Long-term terrestrial carbon dynamics in the Midwestern United States during 1850-2015: Roles of land use and cover change and agricultural management. *Global Change Biology*, *24*(6), 2673–2690.

Yu, Z., Lu, C., Tian, H., & Canadell, J. (2019). Largely underestimated carbon emission from land use and cover change in the conterminous U.S. *Global Change Biology*, *25*(11), 3741–3752. https://doi.org/10.1111/gcb.14768.

Yu, Z., Lu, C., Hennessy, D. A., Feng, H., & Tian, H. (2020). Impacts of tillage practices on soil carbon stocks in the US corn-soybean cropping system during 1998 to 2016. *Environmental Research Letters*, *15*(1), 14008.

Zhang, J., Felzer, B. S., & Troy, T. J. (2016). Extreme precipitation drives groundwater recharge: the Northern High Plains Aquifer, central United States, 1950–2010. *Hydrological Processes*, *30*(14), 2533–2545. https://doi.org/10.1002/hyp.10809

Zhang, J., Lu, C., Feng, H., Hennessy, D., Guan, Y., & Mba-Wright, M. (2021). Extreme climate increased crop nitrogen surplus in the United States. *Agricultural and Forest Meteorology*, *310*. https://doi.org/10.1016/j.agrformet.2021.108632.

Zhang, J., Cao, P., & Lu, C. (2021). Half-century history of crop nitrogen use efficiency budget in the conterminous United States: Variations over time, space and crop types. *Global Biogeochemical Cycles*, e2020GB006876. https://doi.org/10.1029/2020GB006876

Zheng, W., Wang, S., Tan, K., & Lei, Y. (2020). Nitrate accumulation and leaching potential is controlled by land-use and extreme precipitation in a headwater catchment in the North China Plain. *Science of The Total Environment*, *707*, 136168.